Development and Validation of a Generic Finite Element Ribcage to be used for Strain-based Fracture Prediction

(article starts on next page)

Development and Validation of a Generic Finite Element Ribcage to be used for Strain-based Fracture Prediction

Johan Iraeus, Bengt Pipkorn

Abstract   Finite element human body models, comprising detailed anatomical descriptions, can complement anthropomorphic test devices (ATDs) in the development of new restraint systems. Human body models (HBMs) can evaluate injury on tissue level, i.e. rib strain can be used to evaluate the risk of rib fracture, although the HBM must accurately predict the rib strain distribution to be effective. Current HBMs are not validated for rib strain, and it remains unknown if any represent an average-shaped ribcage. Thus, a new generic ribcage was created, representing an average male, based on a combination of averaged geometrical and material data from in-vivo and in-vitro datasets. The ribcage was incorporated into the THUMS AM50 Version 3, resulting in the SAFER HBM Version 9. Validation of ribcage kinetic, kinematics and strain distribution was carried out at three levels of complexity: anterior-posterior rib bending tests; rigid impactor table-top test; and a 40 km/h frontal sled test. The rib strains in the single rib load case were predicted within ± one standard deviation for 91% of the measuring points. The biofidelity for the rib strains in the table-top and sled test load cases was deemed 'fair' using CORA analysis. This study is an important step in the development and validation process of strain-based rib fracture criteria for HBMs.

Keywords   Finite element, Human body model, Ribcage, Strain, Validation.

I.   INTRODUCTION

Currently, anthropomorphic test devices (ATDs) still represent the main tools in the occupant restraint systems development process. For ATDs injury is evaluated based on measurements obtained from accelerometers, angular rate sensors, force transducers or potentiometers in combination with injury risk curves. Chest injury is evaluated based on measurements in one loading direction, i.e. longitudinal chest compression in the Hybrid III and THOR frontal crash test dummies, or lateral chest compression in the EuroSID and WorldSID crash test dummies. Finite element (FE) human body models (HBMs) can be used to complement ATDs. Several studies have shown that the biofidelity of HBMs is higher than that of ATDs [1,2]. A further advantage of HBMs, which comprise detailed anatomical descriptions, over ATDs is that injury can be evaluated on tissue level, which facilitates omnidirectional injury prediction. Rib axial strain has been shown to correlate with fracture location in a variety of load cases [3], and may be a potential candidate for thorax tissue-based injury criteria. In [4] a framework was presented that use the ultimate strain as measured in tensile coupon tests, together with simulation based strain predictions to estimate risk of rib fractures. However, when used in this way, it is essential that the HBM accurately predicts rib strain, i.e. that the model is validated for strain.

The two major HBMs of today, representing average-sized males, are the Total Human Model for Safety (THUMS) AM50 [5] and the Global Human Body Model Consortium (GHBMC) M50-O model [6]. These models are based on subject-specific data [7-10]. The subjects were selected based on external measurements, although whether rib or ribcage dimensions were also taken into consideration in the selection process has not been reported. Ribcage and rib cross-sectional geometry will most likely influence the rib strain distribution.

Until today, HBM thorax validation has been focused on force-deflection response rather than strain measurements [7,11-15]. Rib strain validation have not been published for any of the current HBMs. However, in [7] (THUMS AM50) and [16,17] (GHBMC M50-O) the predicted number of fractured ribs (based on strain based element elimination) have been compared to the actual number of fractured ribs in the PMHS tests. For both models, the number of predicted fractured ribs was underestimated. This may indicate that the models do

J. Iraeus (e-mail: johan.iraeus@chalmers.se; tel: +46 31 772 13 66) is a researcher at Chalmers University of Technology in Sweden.
B. Pipkorn is Director of Simulation and Active Structures at Autoliv Research and Adjunct Professor at Chalmers University.

not predict strain correctly in these load cases.

As it remains unknown if any of the current HBMs truly represents an average-sized ribcage geometry, it was decided to create a generic, average-sized ribcage, based on published data, and to validate it to physical tests, including strain data. The rib response should be valid at different complexity levels, from a single rib up to a complete HBM. The research question is, therefore: can a generic ribcage model, based on averaged geometrical and material data, predict rib strains obtained in physical tests at different levels of complexity, from single rib bending and table-top test up to full PMHS sled tests?

II. METHODS

In-vivo datasets produced from clinical Computer Tomography (CT) images replicate the entire ribcage, and thus represent a feasible data source for creating statistical regression models describing the entire ribcage shape [18-21]. However, due to the small rib cross-sectional dimensions, clinical CT tends to overestimate these dimensions [22]. Instead, in-vitro or micro-CT can be used to quantify the cross-sectional dimensions. The generic ribs in this study were developed based on a combination of in-vitro and in-vivo datasets, described in detail below. After assembling all ribs into a ribcage, the ribcage was incorporated into the THUMS AM50 Version 3 model. This particular HBM was chosen because it has been efficiently implemented, predicting whole-body kinematics, at a rather low CPU cost. Other body regions of the THUMS AM50 Version 3 model were also updated and the final model is hereafter referred to as SAFER HBM Version 9. More details of the generic ribcage are presented below, and information about the updates of the other body parts can be found in Appendix A.

The model validation was carried out in several stages of increasing complexity: anterior-posterior single rib bending [23], table-top test using a rigid impactor on a denuded chest [24], as well as a belted occupant in a 40 km/h frontal sled test [25]. This particular set of reference tests was selected as it includes measuring of rib strains in addition to kinematic and kinetic responses. (Further details are given in the corresponding sections below.) Evaluation of time signals was carried out by comparing FE simulation predictions to physical test results using CORA 3.6.1 [26]. If not stated otherwise, standard CORA settings were used.

Development of a Generic Ribcage

Generic ribs 1–12 were created in four steps, as outlined in Fig. 1. First, 11 elliptical cross-sections were defined along a line representing the rib centre line. Next, the cortical thickness was defined for each ellipse at 16 points along the perimeter. The data for the elliptical half axes, the length of the centre line, as well as the cortical thicknesses were based on the dataset presented in [27]. The points were connected to define the periosteal and endosteal surfaces. Both the cortical and the trabecular bone were meshed using hexahedral elements, and the subsequent step involved converting the cortical hex elements into thin quad shell elements, placed halfway between the periosteal and endosteal surfaces. In this process the thickness of the solid elements was kept as nodal thicknesses in the shell element definitions, thus keeping the variation in cortical thickness defined in the second step. The average shell element side length was 2.5 mm and the average solid element side length was 2.6 mm. The final step involved morphing each rib into the final shape, based on the statistical ribcage model defined in [19]. The parameters for the statistical model were adjusted to be representative of a 40yo male with a stature of 1,770 mm and a BMI of 25. The morphing procedure defined the curvature and twist of each rib, stretching the ribs to conform to the statistical ribcage model while simultaneously maintaining the rib cross-section from the first step. An isotropic plasticity material model (LS-DYNA MAT24) was used for both the cortical and the trabecular bone. Averaged material parameters for the cortical bone were defined by reanalysing the data in [28,29], which resulted in an average Young's modulus of 14.7 GPa, an average yield stress of 100.7 MPa and an average hardening modulus of 1.94 GPa. The material properties for the trabecular bone were obtained from [30,31], with a Young's modulus of 0.04 GPa, a yield stress of 1.8MPa, and a hardening modulus of 0.032 GPa. All solid elements were defined as LS-DYNA solid element Formulation 1, with hourglass Type 2, and the shell elements were defined as LS-DYNA shell element formulation 16, with hourglass Type 8.
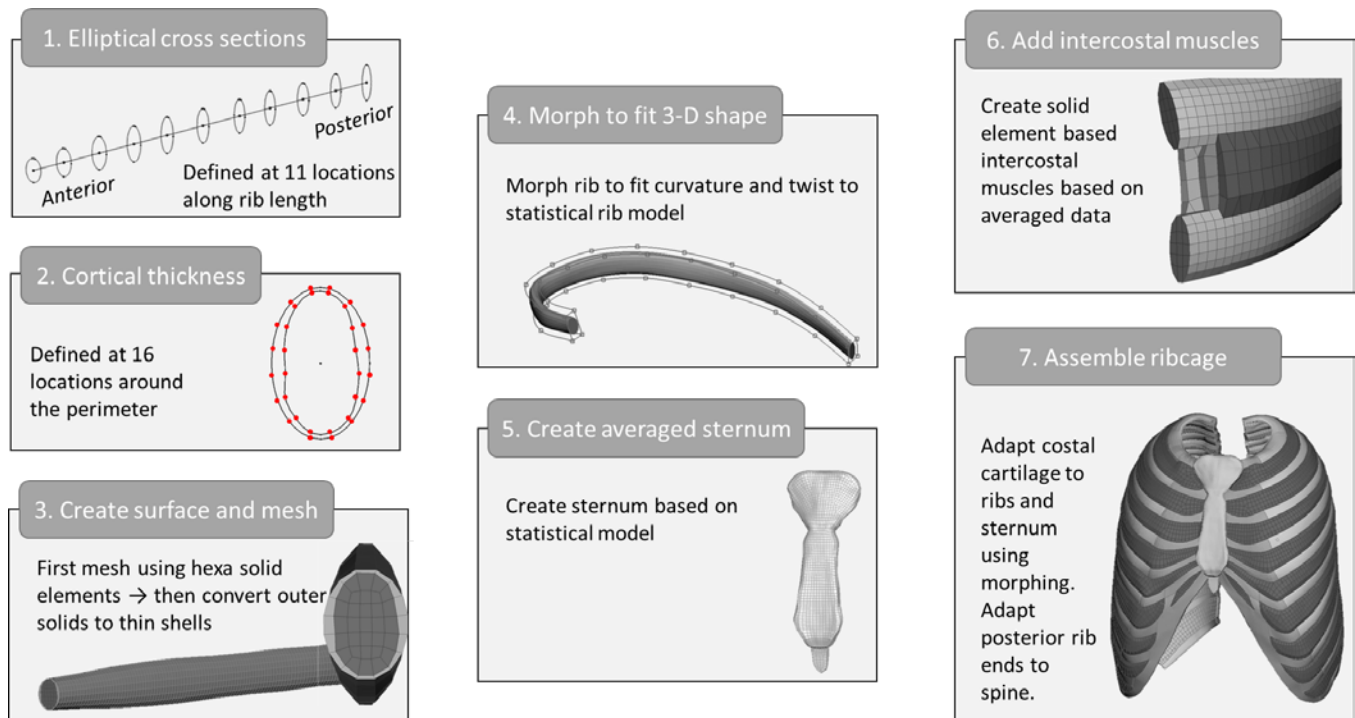
Fig. 1. Procedure to create an average-sized generic ribcage based on averaged data.

The sternum geometry for a 40yo male was defined according to the statistical model defined in [32], with the addition of a 20 mm long Xiphoid process. A CAD surface was fitted onto the data points. This surface was defined as the mid surface of the cortical bone and was meshed using quad shell elements with a uniform thickness of 1 mm. The interior was filled with solid elements representing the trabecular bone. The average shell element side length was 2.5 mm and the average solid element side length was 2.7 mm. The same material model and material parameters as used in THUMS AM50 Version 3 were used for both the cortical and the trabecular bone.

The intercostal muscles (IMs) were modelled with three equally thick layers of solid elements, representing the innermost, internal and external layers of the muscles. The total thickness of the muscles was based on internal analysis performed at the University of Michigan International Center for Automotive Medicine (ICAM) in the USA. In this analysis, live subject CT images were resliced along 3D curves set up halfway between pairs of inferior/superior ribs, producing new image strips that cut across the intercostal space. Intercostal muscle group borders were drawn by operators, and the thickness between these borders facilitated observation of local muscle thickness. This thickness was then predicted across the chest for a typical male subject through the regression method. The IM material test data defined in [33] were used to define material parameters for LS-DYNA material model MAT181 [34].

The final step involved connecting the ribs and intercostal muscles to the sternum by morphing, aligning and re-meshing the THUMS AM50 Version 3 costal cartilage to fit the new geometries and meshes. The original THUMS ver. 3 material model and parameters for the costal cartilage were kept. The whole ribcage was then incorporated into the THUMS AM50 Version 3 by aligning the rib posterior ends to the thoracic vertebras. In this process some ribs were morphed locally to remove mesh intersections in-between the ribs and the spine. Finally, all ligaments, 1-D muscle elements were reattached to the new ribcage and the surrounding soft tissues (flesh, lungs and abdomen) were morphed to fit the updated geometry. In this process, the original THUMS ver. 3 modelling technique and material parameters of the costovertebral and the costotransverse joints were kept.

Validation of Single Ribs

FE models of the anterior-posterior rib bending setups for ribs 2–10 corresponding to [23] (test series two and three) were created, an example of which can be seen in Fig. 2. The generic rib ends were constrained in the end pots. The end pots were then constrained in all degrees of freedom (DOF), except for the out-of-plane rotation to the anterior and posterior fixtures. The posterior end was fixed in space while the anterior end was given a prescribed velocity of 1 m/s. The anterior end was offset laterally to the posterior end. The magnitude of this

offset was computed, separately for each rib level, as the average of the physical tests at that rib level. Posterior reaction force and element strains (the local element coordinate axis directed along the rib length axis) at the positions of the six strain gauges (SG1-6) were measured and compared to the physical test results. CORA scores for the reaction forces of each rib were calculated by comparing the FE predictions to the average of the test corridors defined in [13]. As, the current model do not include modelling of rib failure, the end of the CORA evaluation range for each rib level were selected as the deformation when the first of the ribs, used to design the test corridors, failed. The raw test curves can be seen in [12]. Thus, the CORA evaluation range was 5 mm to 30–45 mm deformation for ribs 3–10 and 2 mm to 10 mm deformation for rib 2.

The FE peak strain predictions for each strain gauge 1–6 were compared, for each rib, to the average test result plus/minus one SD, as reported in [23]. It was not possible to perform a CORA analysis for the rib strains as time histories had not been reported.
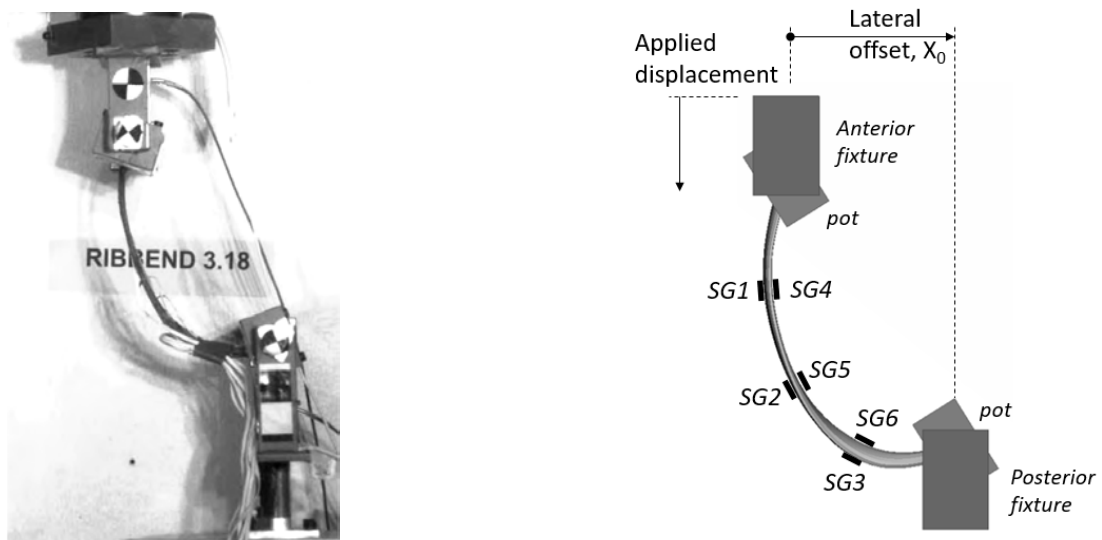

Fig. 2. Anterior-posterior dynamic rib bending test. *Left*: rib bend 3.18, test of rib number 10 (adopted from [23]). *Right*: FE simulation model of anterior-posterior rib bending test of generic rib number 10. SG1-6 marks the positions of the six strain gauges.

Validation of the Complete Ribcage – Table-top test

The validation of the generic ribcage, on component level, was carried out by comparing the FE predictions to kinematics, kinetics and rib strains in physical table-top tests presented in [24,35]. In this test setup the sternum of two PMHS (subject 4 aged 52yo and subject 5 aged 67yo) was impacted with a rigid impactor (covered with rubber) at the level of the 5th rib, as outlined in Fig. 3. In the physical test "natural" rubber was used. This was modelled as a Mooney-Rivlin rubber with shore hardness 65. As in the physical test, the impactor was attached to the loading rod using a ball joint. The impactor speed was 1 m/s and the maximum stroke was 80 mm. In the physical tests the spine, from T1 to L5, was supported by wood screws, preventing lateral, superior/inferior and posterior motion. This was incorporated into the FE model by constraining each vertebrae T1 to L5 to the rigid table. The rib kinematics were evaluated by comparing the FE model rib displacement to eight Vicon® (Vicon Motion Systems Ltd, UK) markers at corresponding positions in the physical tests. Half of the markers were placed on the right ribs and half on the left ribs (at levels 3, 5, 6 and 7/8). The FE model rib strain predictions were evaluated by comparing shell element strains (the local element coordinate axis directed along the rib length axis) to the laterally positioned strain gauges (at ribs 3–10). CORA scores were calculated by comparing the FE predictions to the results of the two physical tests, HSC 4.8 (last test of subject 4) and HSC 5.8 (last test of subject 5). The range for the CORA evaluation was 10 ms to 90 ms for impactor force and kinematics. However, as some rib strain signals were affected by rib fractures, the upper limit of the range for rib strain evaluation was decreased to 75 ms. The CORA weighting factors of the kinematic components were set proportionally to the peak magnitude of each test signal.

Fig. 3. Denuded thorax indentor impacts at mid sternum (centre located at Rib 5). *Left*: pre-test 4.8 (adopted from [35]). *Middle*: pre-test 5.8 (adopted from [35]). *Right*: corresponding simulation model setup. The location of the strain gauges is roughly on one line along the edge of the denuded flesh.

Validation of the Complete Model – Sled Test

The validation of the ribcage on complete HBM level was carried out by comparing the SAFER HBM Version 9 simulation results in a 40 km/h front sled test environment to the results presented in [25]. The test setup, commonly referred to as Gold standard, can be seen in Fig. 4. In this setup the PMHS was seated on a rigid steel plate with additional constraints to the feet and knees, while the thorax was restrained using a standard three-point seatbelt. The torso angle, measured between the greater trochanter and the 1st thoracic vertebral spinous process, was adjusted to match the PMHSs in the physical tests. The seat belt routing was adjusted to conform to the PMHS test setup, with an upper shoulder belt angle of 26° to the horizontal plane, and an angle of 51° in the frontal plane. Results used to validate the FE model were shoulder-belt force, kinematics of the head, T1, T8 and acromion (measured using Vicon®), and rib strains measured at nine locations on ribs 3, 5 and 7. The range used for the CORA calculations was 20 ms to 120 ms for all signals. The CORA weighting factors of the kinematic components were set proportionally to the peak magnitude of each test signal.

Fig. 4. Front sled test 40 km/h. *Left*: PMHS 1,358 (adopted from [25]). *Right*: corresponding FE simulation model.

III. RESULTS

Validation of Single Ribs

As can be seen in Table I, the CORA analysis of the reaction forces for ribs 2–10 produced CORA scores ranging from 0.409 to 0.779, corresponding to marginal to good biofidelity, with an average CORA score of 0.639. Comparing the rib force signals to the test corridors, it was observed that the simulation predictions are within

the corridors, except for deformations up to 30 mm for ribs 6 and 7, and for deformations over 40 mm for rib 9 (see Fig. B1 in Appendix B).

Ninety-one percent (49 out of 54) of the predicted rib strains are within one SD of the physical test results (see Fig. B2 in Appendix B). Of the five predictions outside the ±1 SD, most are right on the border.

TABLE I
CORA SCORES SINGLE RIB KINETIC VALIDATION

Result component	CORA score	Rating (ISO/TR 9790)
Rib 2	0.775	Good
Rib 3	0.717	Good
Rib 4	0.596	Fair
Rib 5	0.706	Good
Rib 6	0.429	Marginal
Rib 7	0.409	Marginal
Rib 8	0.586	Fair
Rib 9	0.779	Good
Rib 10	0.756	Good

Validation of the Complete Ribcage – Table-top Test

As seen in Table II, the CORA scores for the evaluation of the table-top impactor force was 0.574, for the kinematics 0.702 and for the rib strains 0.505, corresponding to fair to good biomechanics ratings. Detailed results can be seen in Appendix C, where Fig. C1 shows the impactor force responses, Fig. C2-C4 the rib kinematic responses, and Fig. C5-C6 the rib strain responses.

TABLE II
CORA SCORES TABLE-TOP VALIDATION

Result component	CORA score	Rating (ISO/TR 9790)
Impactor forces	0.574	Fair
Kinematics	0.702	Good
Rib strains	0.505	Fair

Validation of the Complete Model – Sled Test

A comparison of the kinematics in the sled test load case can be seen in Fig. 5. The major difference is more axial rotation of the THUMS HBM Version 9 upper body at 140 ms compared to this PMHS.
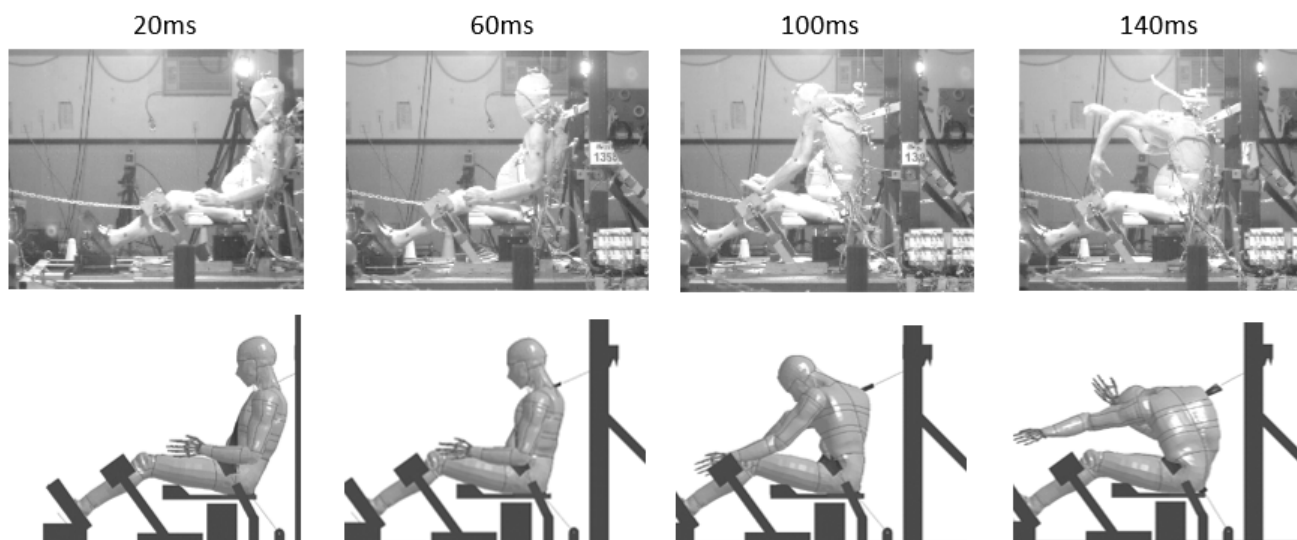

Fig. 5. Overall kinematics of the SAFER HBM Version 9 compared to one PMHS (test 1358) in the sled test load case. The PMHS images are adopted from [25].

The CORA score for the sled test belt forces was 0.709, the kinematics 0.660 and the rib strains 0.444, corresponding to fair to good biomechanics rating (see Table III). More results can be found in Appendix D, where Fig. D1 shows the belt force results, Fig. D2-D3 the kinematics results, and Fig. D4 the rib strain results.

TABLE III
CORA SCORES SLED TEST VALIDATION

Result component	CORA score	Rating (ISO/TR 9790)
Belt forces	0.709	Good
Kinematics	0.660	Good
Rib strains	0.444	Fair

IV. DISCUSSION

A generic ribcage representing an average-sized male was created based on averaged data. Rib cross-sectional properties as well as cortical thicknesses were based on a detailed dataset of seven elderly Korean men [27]. The overall rib sizes and shapes (excluding cross-sections) were based on a statistical regression model [19]. This regression model was in turn based on clinical CT scans of 89 individuals, essentially evenly distributed over the sexes, statures (1.5–2.0 m), BMIs (16–55 kg/m^2) and ages (18–89 years). The sternum shape was based on a regression model based on 330 individuals, essentially evenly distributed over the sexes and ages (0–97 years). These datasets are based on individuals of different ages, originating from different continents, and thus it is not possible to state what population average the generic model represents. In particular, the target age for the regression shape models was selected to be 40yo, while the cross sectional and cortical thickness data was based on subjects with an average age of 71 years. The age related changes of rib cross sectional dimensions have been studied extensively [36-40]. The results are consistent, showing that the cross section dimensions peaks around 20 years of age, then drops until 30 years of age, and are more or less constant over the rest of the life span. In addition, the interpersonal variability is very large, making the age related relationships very weak. Thus, it was decided not to age adjust the rib cross sectional dimensions for this study.

In addition, the small sample used to create the average cross-sectional and cortical thickness dimensions leaves some uncertainty about the validity of the average properties of these dimensions. However, the dataset in [27] is currently the best data source, including detailed measurements of both rib cross-sectional data and cortical thicknesses from the same individuals. Cortical bone mapping is a promising technology suitable for creating much larger, reasonably accurate data-sets measuring rib shape, rib cross-sectional dimensions and estimating cortical thickness on the same individuals, which has been applied to ribs in certain recent studies [41,42].

Rib strain validation is the main focus of the current study. Generally, there are very few validation data sets including rib strain measurements, which means that there is hard to find tests matching the desired target population. The average age for the PMHSs used as validation data was 53yo (31-62) for the single rib tests, 60yo (52-67) for the table-top test, and 53yo (49-57) for the sled test. Studies have shown that the structural properties of ribs are correlated to age [40,43] with lower stiffness and lower peak displacement for elderly. In particular, the ultimate strain and strain energy density is negatively correlated with age [44]. However, in this study rib failure properties are not studied. Instead, the predicted rib strain is compared to the measured strain at the same deformation or external load, meaning that only the age related change in stiffness might be a concern. In [40] the authors found "a negative trend in the adult group, although not practically significant", when comparing the age related stiffness trend to the interpersonal variance. Thus, considering the small number of subjects in the validation data sets it was decided not to age adjust the validation data.

Generally, a prerequisite to strain validation is correct modelling of kinematics and kinetics. For the single ribs the kinetic CORA rating ranged from marginal to good biofidelity, with best results for the upper and lower ribs. However, for this test setup, marginal kinetic rating (meaning that the rib force-deflection response does not match the physical test) does not necessarily mean that the strain prediction capability has to be poor, as the

loading in this setup is displacement controlled. In a displacement controlled rib test the maximum strain will depend on the maximum displacement, while the maximum force will also depend on the rib stiffness. The rib strain was predicted within ±1 SD in 91% of the measuring points, with the predictions outside the ±1 SD range concentrated to the upper ribs (1–5).The force-deflection properties of the GHBMC ribs have previously been validated [13] using the same data set. The average CORA score was 0.76, which is higher compared to the current study. However, it should be noted that both force and deflection was normalized in [13], making a direct comparison CORA scores hard.

The table-top load case can also be considered displacement controlled. However, in this load case the impactor is not connected to the ribcage and can rotate and slide relative to the ribcage. This was also observed in test HSC 5.8, where the impactor slid along the sternum. Figure 3 shows that the sternum of the PMHS used in test HSC 5.8 was significantly shorter and sloped downwards in the superior direction. In the table-top load case, the stiffness and inertia effects of the intercostal muscles and the front portion of the visceral organs are added to the denuded ribcage force response, enhancing its complexity. The CORA analysis showed that the biofidelity of the impactor force prediction was fair, while the prediction of ribcage kinematics showed good biofidelity. The biofidelity for the rib strains was deemed to be fair. Examining the rib strain results closer (see Appendix C (Fig. C5-C6)), it can be noticed that the upper ribs are more in agreement with test results compared to the lower. In fact, if the CORA analysis were only carried out on the true ribs (here 3–7), the CORA rating for the rib strains would improve from fair to good. For the lower ribs the force from the impactor must be transferred through a large portion of costal cartilage. This, in combination with the good CORA rating for the low ribs in the single rib load cases (Table I), indicates that the costal cartilage in the FE model does not transfer the loads correctly.

The third and most complex validation load case was the sled test. In this load case the whole thorax model, including all surrounding soft tissues, was evaluated. In this load case the thorax loading is realistic in the sense that it is inertia-loaded and the restraint is a standard three-point seat belt. The CORA analysis for the belt forces and the upper body kinematics showed good biofidelity. However, as can be seen in Fig. 5, the simulation model predicts more upper body axial rotation comparison to the PMHS. It is assumed that this is the reason the FE model predicted negative Y-translation for T1 down to L4, while the PMHS test show positive or zero Y-translation. The root cause is most likely the PMHS's more pronounced belly, pushing the lower left part of the shoulder belt higher up on the thorax. This also means that the shoulder belt possibly interacts with the ribs in a different way in the simulation model, and in particularly on the lower left side. The strain time histories for the lower left ribs, seen in Appendix D (Fig. D4), shows that the strain magnitude prediction are within the physical test result variation. However, the predicted strain onset shows a phase shift compared to the physical test results. It is unclear if this phase shift is a result of the excessive rotation or that the pronounced belly initially unloads the ribs, and also if strain at other measuring points was affected. In addition, the local strain compression peaks around 50ms, seen for some ribs in the PMHS tests, are not replicated by the HBM. In [25] the authors attributes this phenomena to the asymmetrical belt loading and inertial loading of the ribcage and the underlying organs. The HBM presented here has a simplified modelling of the visceral organs and modelling/attachment of the subcutaneous fat/muscles, preventing the inertia from being properly transmitted to the ribs during the early loading. The overall CORA score for the rib strains in this load case was 0.444, which corresponds to fair biofidelity. In general, the strain predictions of the generic ribcage show reasonable agreement with the results of the physical tests for the load cases analysed in this study. The GHBMC kinematics in a frontal sled environment (DV 12 and 24kph) have been evaluated in [45]. The average CORA scores were 0.61 and 0.65 which can be compared to the kinematic CORA score of 0.66 in the current study.

The next step will be to use the model to predict the risk for rib fractures, i.e. using the probabilistic framework presented in [4]. This method uses the first principle rib strain in the cortical bone to estimate fracture risk. In addition, the generic ribcage model presented in this study is suitable to use as a baseline model for HBM morphing. Using the method outlined in [46], the rib cross sectional dimensions, as well as overall rib shape will be morphed based on anthropomorphic data like age, sex, stature and BMI. The model, and the strain predictability, should then be further validated using datasets of non-average subjects.

A limitation of the current study is that only anterior-posterior load cases, corresponding to frontal impacts, were evaluated. To ensure omnidirectional validity for strain predictions, the validation should be extended to include oblique and lateral load cases. Some datasets, including strain measurements, suitable for such validation have been presented in [3,47-49]. Compared to the total number of published studies that can be used for HBM thorax validation, the number of studies including rib strain measurements is limited. In addition, the strain gauge instrumentation used in most published studies has primarily been included to detect rib fractures, not to capture the strain distribution throughout the rib. Future PMHS testing, to be used for HBM validation, should preferably be carried out with strain gauges developed to give accurate readings in humid conditions, including multiple strain gauges positioned along the ribs, to capture the strain variation along the rib.

Another limitation is that the number of PMHS subjects for the table-top and sled data sets are small, leaving some uncertainty of the representativeness for these tests. Additional validation should be carried out when more data becomes available.

V. CONCLUSIONS

A generic ribcage model was created based on averaged data and validated stepwise at different levels of complexity, from human single rib to whole-body level by means of PMHS sled tests. The rib strain biofidelity was good (91% of the strain predications within one SD) in single rib anterior-posterior bending load cases and fair in the table-top and sled test load cases. This is an important step for the development and validation of strain-based rib fracture criteria for HBMs.

VI. ACKNOWLEDGEMENTS

VII. REFERENCES

[1] Lanner, D., Halldin, P., et al. Evaluation of finite element human body models in lateral padded pendulum impacts to the shoulder. *International Journal of Crashworthiness*, 2010, 15(2):125-142

[2] Park, G., Kim, T., et al. Evaluation of biofidelity of side impact computational surrogates (ES-2re, WorldSID, GHBMC). *Proceedings of the SAE 2014 World Congress & Exhibition*, 2014, Detroit, US

[3] Trosseille, X., Baudrit, P., Leport, T., and Vallancien, G. Rib cage strain pattern as a function of chest loading configuration. *Stapp Car Crash Journal*, 2008, 52:205-231

[4] Forman, J.L., Kent, R.W., et al. Predicting rib fracture risk with whole-body finite element models: development and preliminary evaluation of a probabilistic analytical framework. *Proceedings of the 56th annual AAAM Scientific Conference*, 2012, Seattle, Washington

[5] Toyota Central R&D Labs. INC. "Human Body Models for Injury Analysis THUMS®" Internet https://www.tytlabs.com/tech/thums/index.html. [Date Accessed: 26 Nov 2018].

[6] Elemance. "Virtual Human Body Models" Internet http://www.elemance.com/virtual-human-body-models/. [Date Accessed: 26 Nov 2018].

[7] Shigeta, K., Kitagawa, Y., and Yasuki, T. Development of next generation human FE model capable of organ injury prediction. *Proceedings of the 21st Annual Enhanced Safety of Vehicles*, 2009, Stuttgart, Germany

[8] Iwamoto, M., Nakahira, Y., and Kimpara, H. Development and validation of the total human model for safety (THUMS) toward further understanding of occupant injury mechanisms in precrash and during crash. *Traffic Injury Prevention*, 2015, 16(sup1):S36-S48

[9] Gayzik, F., Hamilton, C., et al. A Multi-Modality Image Data Collection Protocol for Full Body Finite Element Model Development. *Proceedings of the SAE 2010 World Congress & Exhibition*, 2010, Detroit, US

[10] Gayzik, F., Moreno, D., et al. External landmark, body surface, and volume data of a mid-sized male in seated and standing postures. *Annals of Biomedical Engineering*, 2012, 40(9):2019-2032

[11] Iwamoto, M. Development of a finite element model of the total human model for safety (THUMS) and application to injury reconstruction. *Proceedings of the International IRCOBI Conference*, 2002, Munich, Germany

[12] Li, Z., Subit, D., Kindig, M., and Kent, R. Development of a Finite Element Ribcage Model of the 50th Percentile Male with Variable Rib Cortical Thickness. *Proceedings of the thirty-Eight International Worlshop, Injury Biomechanics Research*, 2010,

[13] Poulard, D., Kent, R.W., Kindig, M., Li, Z., and Subit, D. Thoracic response targets for a computational model: a hierarchical approach to assess the biofidelity of a 50th-percentile occupant male finite element model. *Journal of the Mechanical Behavior of Biomedical Materials*, 2015, 45:45-64

[14] Vavalle, N.A., Moreno, D.P., Rhyne, A.C., Stitzel, J.D., and Gayzik, F.S. Lateral impact validation of a geometrically accurate full body finite element model for blunt injury prediction. *Annals of Biomedical Engineering*, 2013, 41(3):497-512

[15] Vavalle, N.A., Davis, M.L., Stitzel, J.D., and Gayzik, F.S. Quantitative validation of a human body finite element model using rigid body impacts. *Annals of Biomedical Engineering*, 2015, 43(9):2163-2174

[16] Schoell, S.L., Weaver, A.A., et al. Development and Validation of an Older Occupant Finite Element Model of a Mid-Sized Male for Investigation of Age-related Injury Risk. *Stapp Car Crash Journal*, 2015, 59:359-383

[17] Schoell, S.L., Weaver, A.A., Vavalle, N.A., and Stitzel, J.D. Age-and sex-specific thorax finite element model development and simulation. *Traffic Injury Prevention*, 2015, 16(sup1):S57-S65

[18] Gayzik, F.S., Mao, M.Y., Danelson, K.A., Slice, D.E., and Stitzel, J.D. Quantification of age-related shape change of the human rib cage through geometric morphometrics. *Journal of Biomechanics*, 2008, 41(7):1545-1554

[19] Shi, X., Cao, L., et al. A statistical human rib cage geometry model accounting for variations by age, sex, stature and body mass index. *Journal of Biomechanics*, 2014, 47(10):2277-2285

[20] Weaver, A.A., Schoell, S.L., and Stitzel, J.D. Morphometric analysis of variation in the ribs with age and sex. *Journal of Anatomy*, 2014, 225(2):246-261

[21] Wang, Y., Cao, L., et al. A parametric ribcage geometry model accounting for variations among the adult population. *Journal of Biomechanics*, 2016, 49(13):2791-2798

[22] Perz, R., Toczyski, J., et al. Evaluation of the geometrical properties distribution along the human ribs using different X-Ray imaging methods. *Proceedings of the international IRCOBI Conference*, 2013, Gothenburg, Sweden

[23] Kindig, M.W. Tolerance to failure and geometric influences on the stiffness of human ribs under anterior-posterior loading, in *School of Engineering and Applied Science*. 2009, University of Virginia, US.

[24] Shaw, C.G., Lessley, D., et al. Quasi-static and dynamic thoracic loading tests: cadaveric torsos. *Proceedings of the proceedings of the IRCOBI conference*, 2007, Maastricht, Netherlands

[25] Shaw, C.G., Parent, D., Purtsezov, S., Shin, J., and Crandall, J.R. Frontal impact PHMS sled tests for FE torso model development. *Proceedings of the proceedings of the IRCOBI conference*, 2009, York, UK

[26] Thunert, C. CORA Release 3.6 User's Manual. 2012, PDB - Partnership for Dummy Technology and Biomechanics: Gaimersheim, Germany.

[27] Choi, H.-Y. and Kwak, D.-S. Morphologic Characteristics of Korean Elderly Rib. *Journal of Automotive Safety and Energy*, 2011, 2(2):122-127

[28] Kemper, A.R., McNally, C., et al. Material properties of human rib cortical bone from dynamic tension coupon testing. *Stapp Car Crash Journal*, 2005, 49:199-230

[29] Kemper, A.R., McNally, C., et al. The biomechanics of human ribs: material and structural properties from dynamic tension and bending tests. *Stapp Car Crash Journal*, 2007, 51:235-273

[30] Kimpara, H., Lee, J.B., Yang, K.H., and King, A.I. Development of a three-dimensional finite element chest model for the 5th percentile female. *Stapp Car Crash Journal*, 2005, 49:251

[31] Zhao, J.Z. and Narwani, G. Development of a human body finite element model for restraint system R&D applications. *Proceedings of the 19th International Technical Conference on the Enhanced Safety of Vehicles*, 2005, Washington D.C., US

[32] Weaver, A.A., Schoell, S.L., Nguyen, C.M., Lynch, S.K., and Stitzel, J.D. Morphometric analysis of variation in the sternum with sex and age. *Journal of Morphology*, 2014, 275(11):1284-1299

[33] Poulard, D. and Subit, D. Unveiling the structural response of the ribcage: contribution of the intercostal muscles to the thoracic mechanical response. *Proceedings of the 24th International Technical Conference on the Enhanced Safety of Vehicles (ESV)*, 2015, Gothenburg, Sweden

[34] LSTC. LS-DYNA Keyword User's Manual. 2015, Livermore Software Technonlgy Corporation: Livermore, California, US.

[35] Shaw, C.G., Lessley, D., and Crandall, J. Quasi-Static and Dynamic Thoracic Loading Tests: Cadaveric Torsos. 2007, Virginia, US: A Report Prepared for NHTSA, Cooperative Agreement No. DTNH22-93-Y-07028.

[36] Sedlin, E.D., Frost, H.M., and Villanueva, A.R. Variations in cross-section area of rib cortex with age. *Journal of Gerontology*, 1963, 18(1):9-13

[37] Epker, B., Kelin, M., and Frost, H. Magnitude and location of cortical bone loss in human rib with aging. *Clinical Orthopaedics and Related Research*, 1965, 41:198-203

[38] Takahashi, H. and Frost, H.M. Age and sex related changes in the amount of cortex of normal human ribs. *Acta Orthopaedica Scandinavica*, 1966, 37(2):122-130

[39] Stein, I. and Granik, G. Rib structure and bending strength: an autopsy study. *Calcified Tissue Research*, 1976, 20(1):61-73

[40] Agnew, A.M., Murach, M.M., et al. Sources of Variability in Structural Bending Response of Pediatric and Adult Human Ribs in Dynamic Frontal Impacts. *Stapp Car Crash Journal*, 2018, 62:119-192

[41] Holcombe, S., Personal Communication

[42] Okoukoni, C., Lynch, S.K., et al. A cortical thickness and radiation dose mapping approach identifies early thinning of ribs after stereotactic body radiation therapy. *Radiotherapy and Oncology*, 2016, 119(3):449-453

[43] Agnew, A.M., Schafman, M., Moorhouse, K., White, S.E., and Kang, Y.-S. The effect of age on the structural properties of human ribs. *Journal of the mechanical behavior of biomedical materials*, 2015, 41:302-314

[44] Albert, D.L., Kang, Y.-S., Agnew, A.M., and Kemper, A.R. A Comparison of Rib Structural and Material Properties from Matched Whole Rib Bending and Tension Coupon Tests. *Proceedings of International IRCOBI Conference*, 2017, Antwerp, Belgium

[45] Arun, M.W., Humm, J.R., Yoganandan, N., and Pintar, F.A. Biofidelity evaluation of a restrained whole body finite element model under frontal impact using kinematics data from PMHS Sled Tests. *Proceedings of IRCOBI Conference Proceedings*, 2015,

[46] Yang, K.-H., "Basic finite element method as applied to injury biomechanics", pages 417-445, Academic Press, 2017

[47] Lopez-Valdes, F., Juste-Lorente, O., et al. Analysis of occupant kinematics and dynamics in nearside oblique impacts. *Traffic Injury Prevention*, 2016, 17(sup 1):131-140

[48] Lessley, D., Shaw, G., et al. Whole-Body Response to Pure Lateral Impact. *Stapp Car Crash Journal*, 2010, 54:289

[49] Miller, C.S., Madura, N.H., et al. PMHS Impact Response in 3 m/s and 8 m/s Nearside Impacts with Abdomen Offset. *Stapp Car Crash Journal*, 2013, 57:387

VIII.   APPENDIX

APPENDIX A

Model updates in SAFER HBM Version 9
In addition to the ribcage updates outlined in the current study, the SAFER HBM version 9 model was also updated in some other body regions as described in this appendix.

Head and neck
The head of the THUMS version 3 model was replaced by the KTH head [A1]. The original skull base was kept, as this matches the neck, and attached to the new skull. All 1-D muscles were replaced with new muscles based on the work in [A2]. The neck flesh and scalp geometry were updated based on the surface geometry of a 50%ile male described in [A3]. The material model for the neck skin was updated according to [A4]. The updated head and neck model can be seen in Fig. A1.
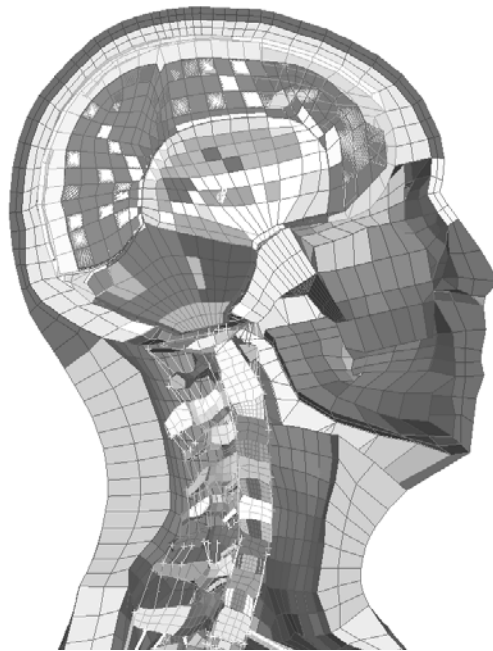
Fig. A1. A section cut through the updated neck and head model.

Lumbar Spine

The lumbar spine was updated according to the suggestions in [A5]. This included geometrical and material updates of the intervertebral ligaments and discs and updated contact definitions to improve biofidelity.

[A1]   Kleiven, S. (2007) Predictors for Traumatic Brain Injuries Evaluated through Accident Reconstructions. *Stapp Car Crash Journal,* 51: pp. 81–114.

[A2]   Ólafsdottir, J. M. (2009) Muscle responses in dynamic events – Volunteer experiments and numerical modeling for the advancement of human body models for vehicle safety assessment. Mechanics and Maritime Sciences, 2009, Göteborg.

[A3]   Reed, M., Parkinson, P., Matthew, B. (2008) Modeling variability in torso shape for chair and seat design. *Proceedings of the ASME*, 2008, Brooklyn, New York, USA.

[A4]   Manschot, J. and Brakkee, A. (1986) The measurement and modelling of the mechanical properties of human skin in vivo—II. The model. *Journal of Biomechanics*, 19(7): pp. 517–21.

[A5]   Afwerki, H. (2016) Biofidelity Evaluation of Thoracolumbar Spine Model in THUMS. Master's Thesis in Biomedical Engineering, Chalmers University of Technology.

APPENDIX B

Extended Results of Single Rib Validation

This appendix includes a comparison of test and simulation time series of single rib load cases. In Fig. B1 posterior end reaction force versus anterior end displacement are compared. In Fig. B2 predicted rib strains are compared to the variation of strains in the physical tests.
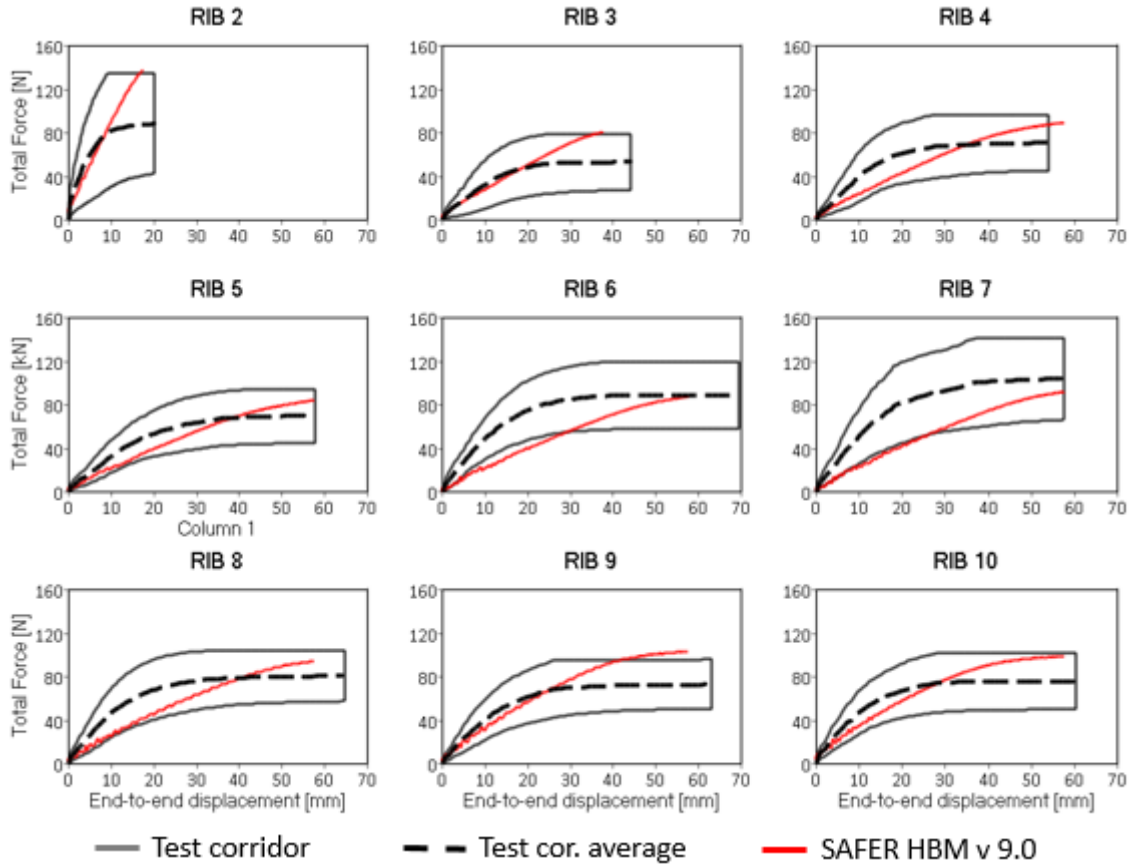
Fig. B1. Comparison of test and simulation reaction forces in the single rib load cases.
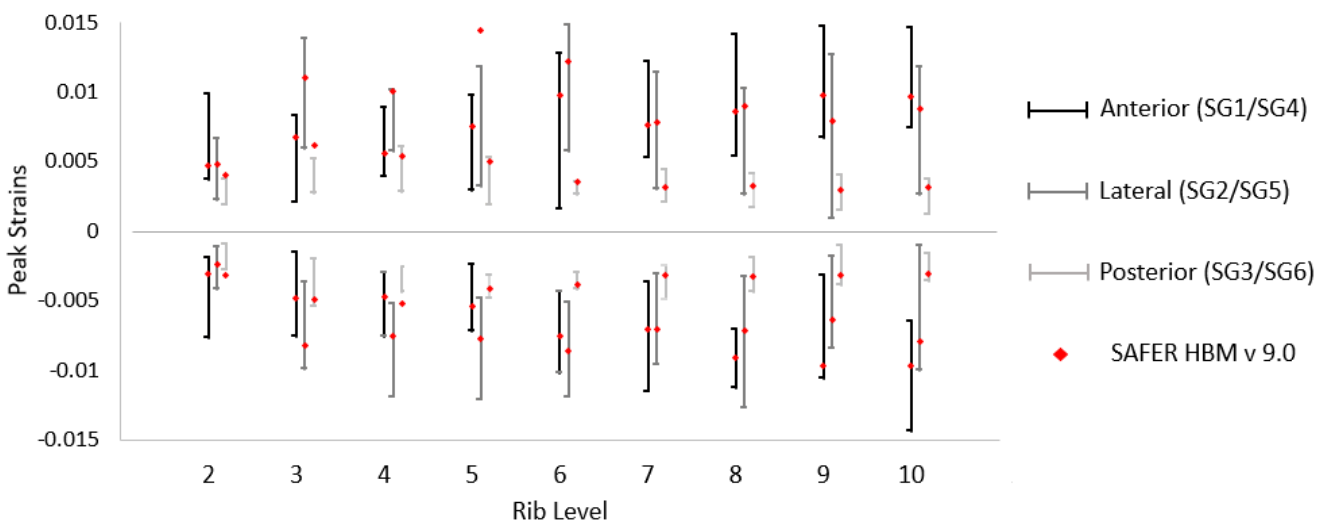
Fig. B2. Comparison of test and simulation rib strain in the single rib load cases.

APPENDIX C

Extended Results of Table-Top Validation

This appendix includes a comparison of test and simulation time series of table-top load cases. In Fig. C1 impactor forces are compared. In Fig. C2-C4 ribcage X, Y and Z kinematics are compared. In Fig. C5-C6 rib strains on the right and left side are compared.
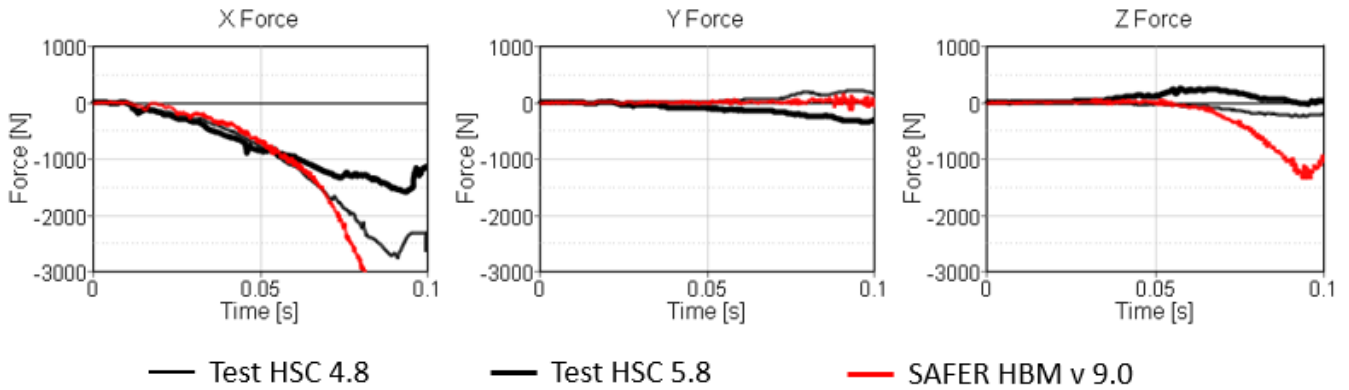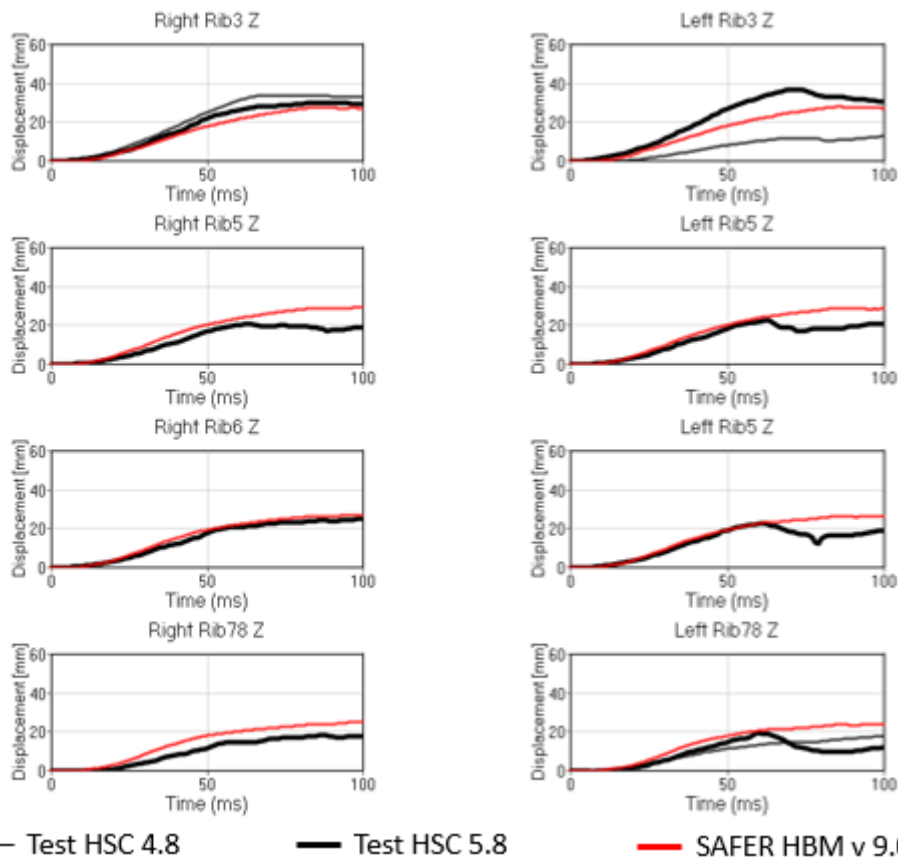

Fig. C1. Comparison of test and simulation impactor forces in the table-top load case.
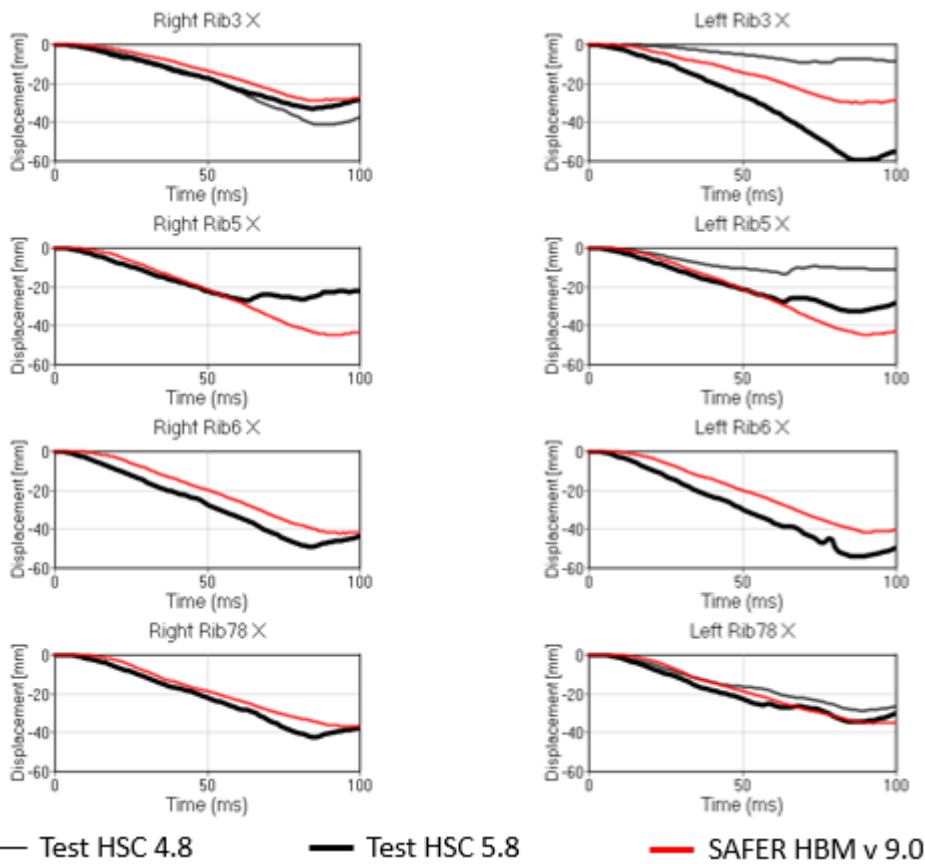
Fig. C2. Comparison of test and simulation Vicon® X-translational kinematics in the table-top load case.
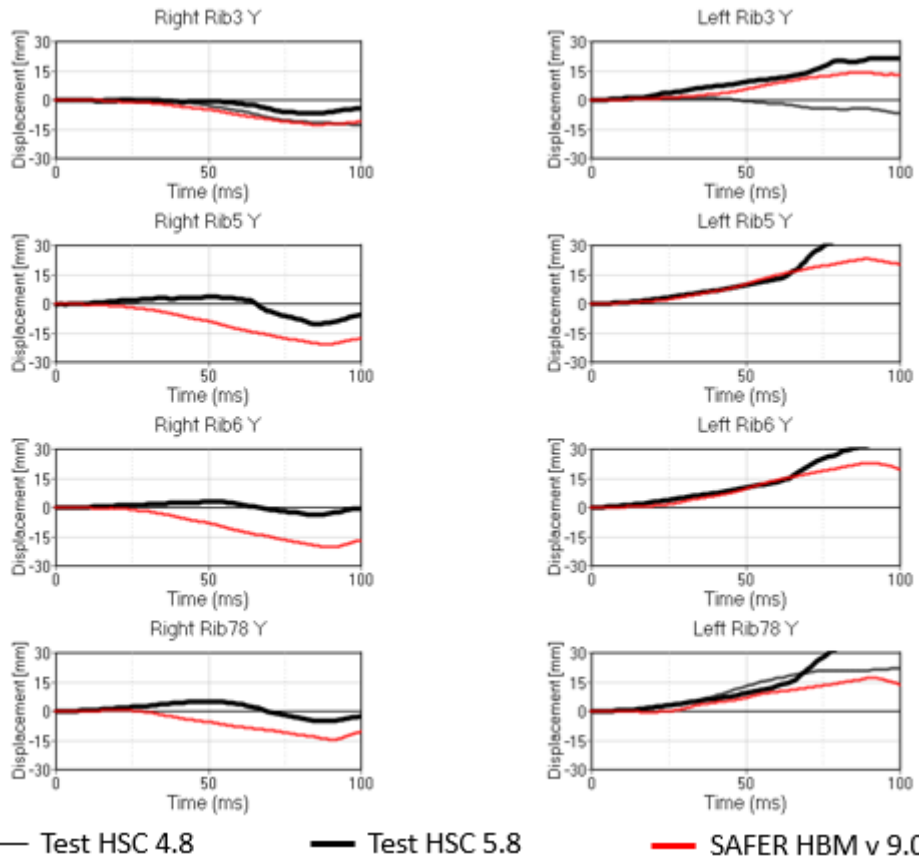
Fig. C3. Comparison of test and simulation Vicon® Y-translational kinematics in the table-top load case.

Fig. C4. Comparison of test and simulation Vicon® Z-translational kinematics in the table-top load case.
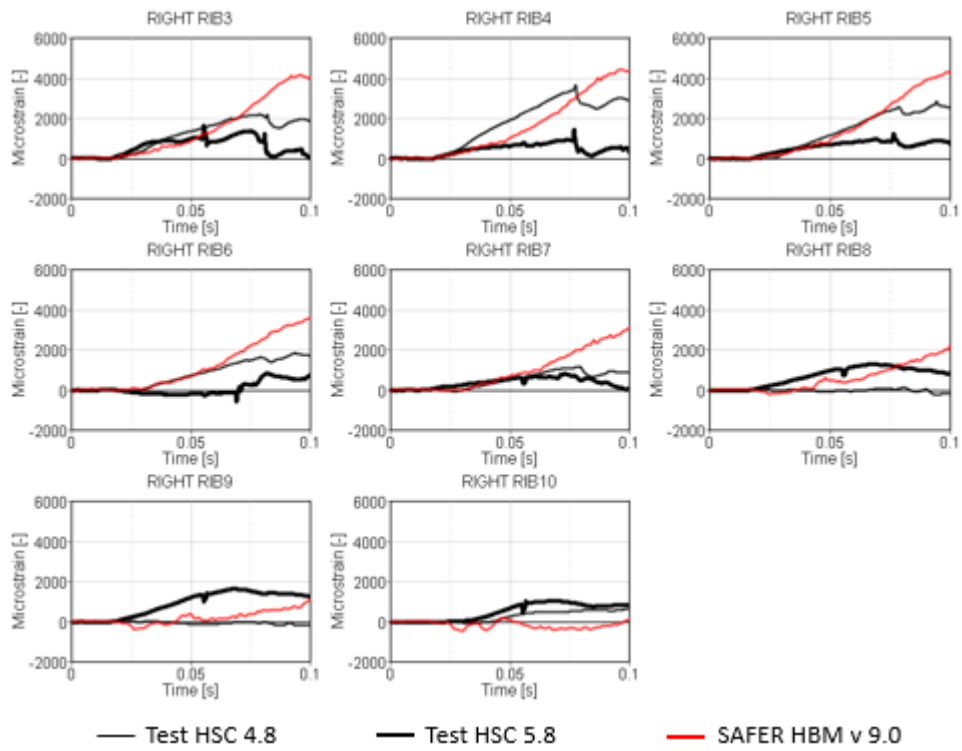
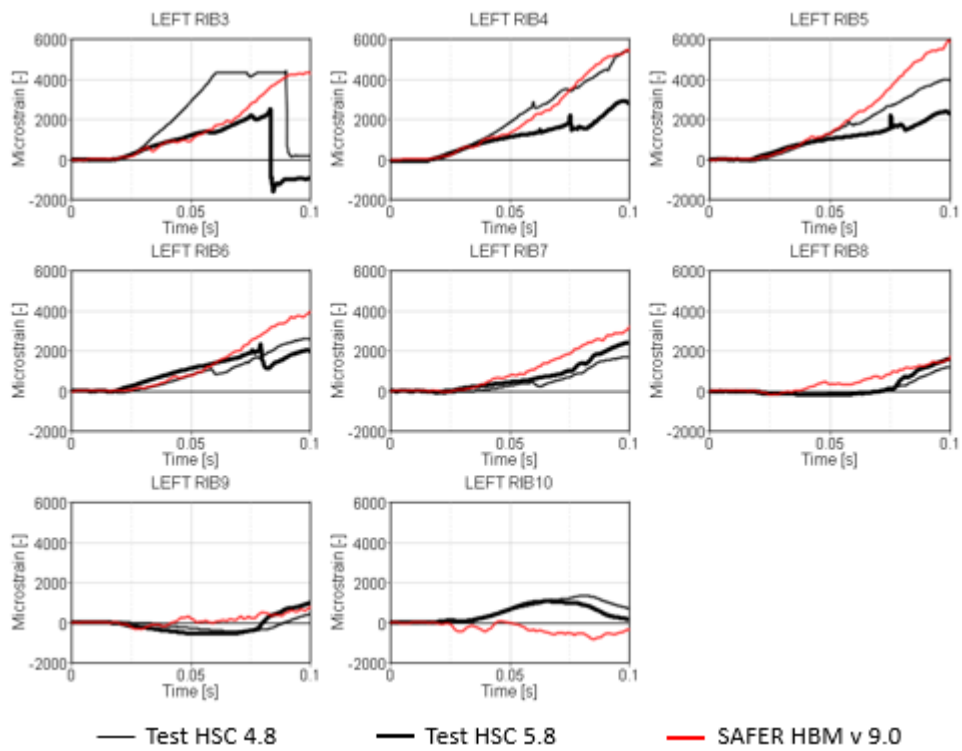Fig. C5. Comparison of test and simulation right rib strains in the table-top load case.

Fig. C6. Comparison of test and simulation left rib strains in the table-top load case.

APPENDIX D

Extended Results of Sled Test Validation

This appendix includes a comparison of test and simulation time series of sled test load cases. In Fig. D1 upper and lower shoulder-belt forces are compared. In Fig. D2 head and thoracic spine kinematics are compared. In Fig. D3 lumbar spine and pelvic kinematics are compared. In Fig. D4 rib strains are compared.
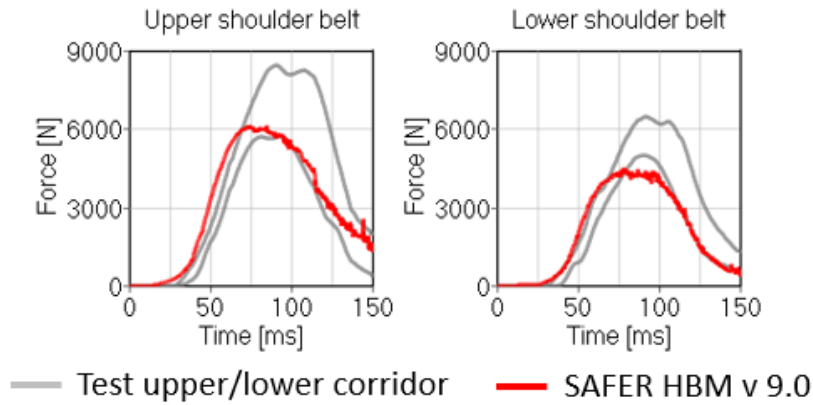
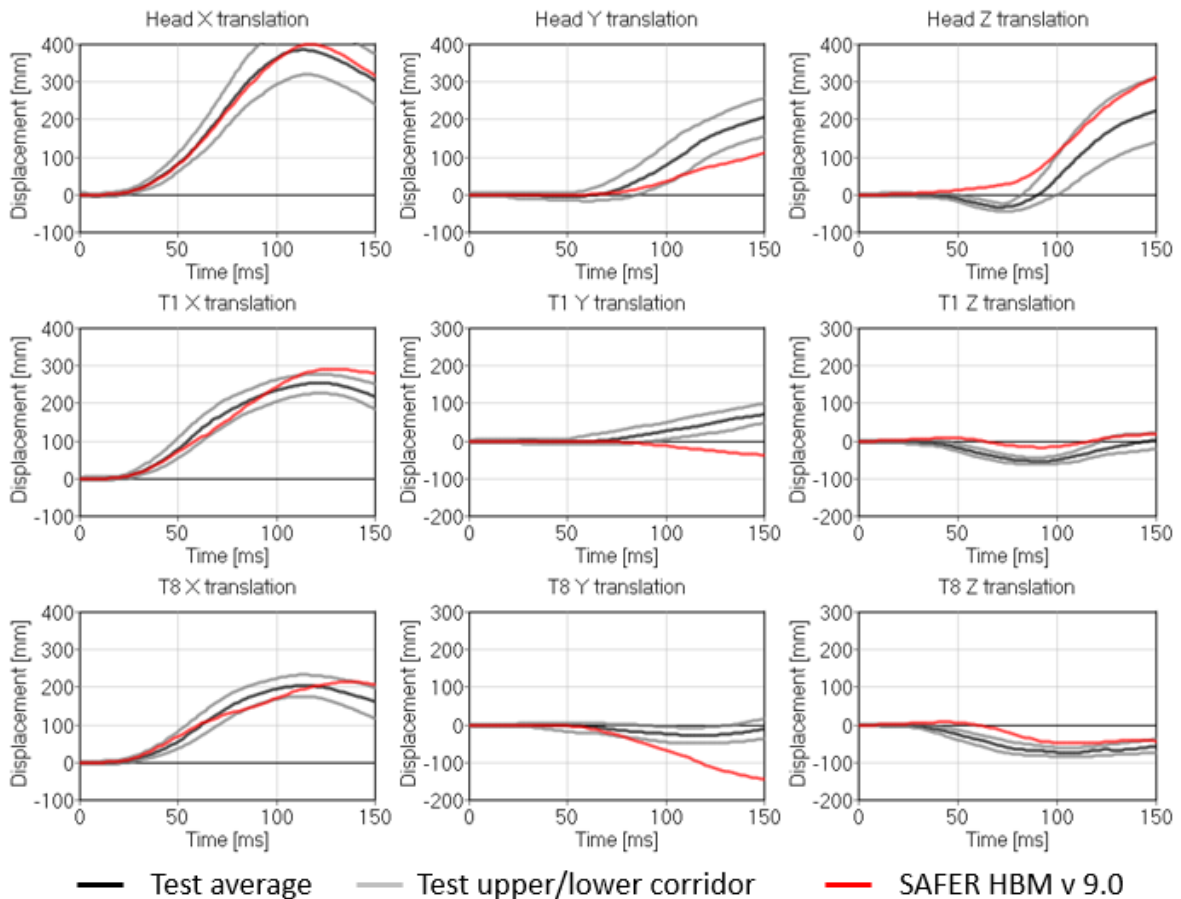Fig. D1. Comparison of test and simulation shoulder-belt forces in the sled test load case.

Fig. D2. Comparison of test and simulation head and thorax kinematics in the sled test load case.
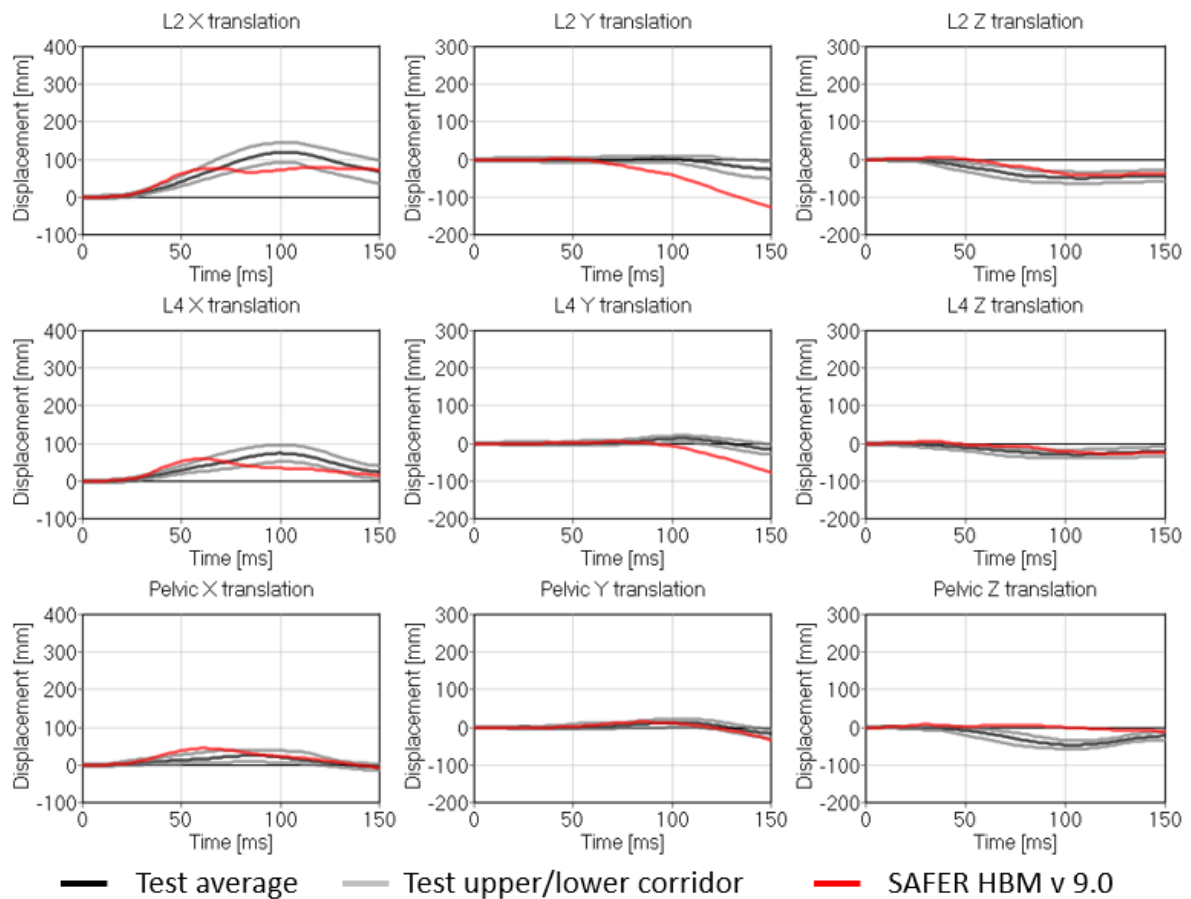
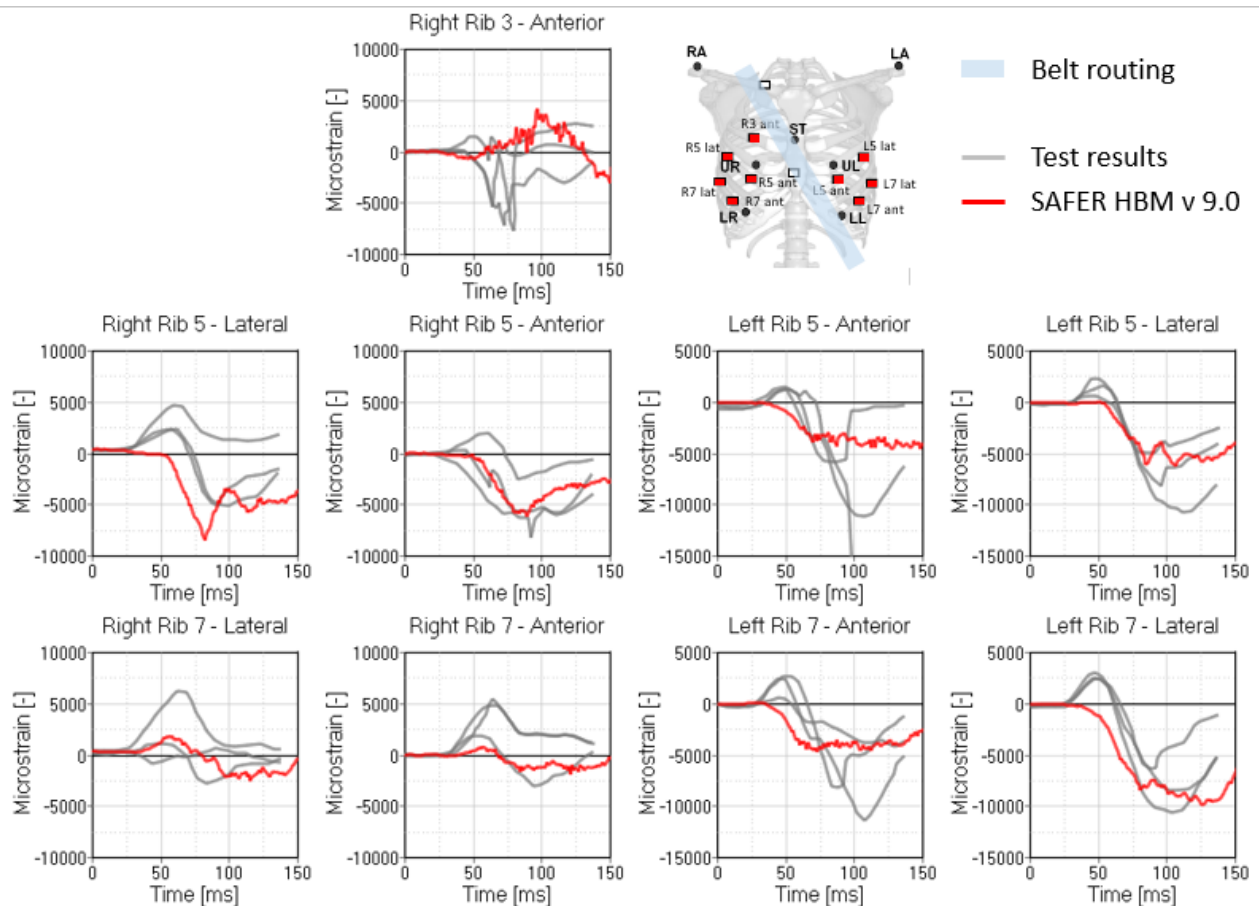Fig. D3. Comparison of test and simulation lumbar and pelvic kinematics in the sled test load case.

Fig. D4. Comparison of test and simulation rib strains in the sled test load case.